Desalination and Water Treatment
www.deswater.com
doi: 10.1080/19443994.2015.1101619

57 (2016) 19540–19556
September

Taylor & Francis
Taylor & Francis Group

Experimental and comparative study of a sea water-cooled surface condenser of LTTD plant with HTRI and Kern method

D. Balaji[a,*], Raju Abraham[b], S.V.S. Phani Kumar[a], M.V. Ramana Murthy[a]

[a]*Department of Ocean Structures, National Institute of Ocean Technology, Chennai, India, Tel. +91 66783359; email: dbalaji@niot.res.in (D. Balaji), Tel. +91 66783349; email: phani@niot.res.in (S.V.S. Phani Kumar), Tel. +91 66783586; email: mvr@niot.res.in (M.V. Ramana Murthy)*
[b]*Department of VMC, National Institute of Ocean Technology, Chennai, India, Tel. +91 66783339; email: dbalaji@niot.res.in*

Received 18 December 2014; Accepted 23 September 2015

ABSTRACT

Low-temperature thermal desalination is a process which involves evaporation of warm surface sea water at 28–29°C inside an evaporator which is maintained at a subatmospheric pressure of around 24–27 mbar [abs] and the resultant vapour is condensed in the condenser using deep-sea cooling water (12–13°C) drawn from a depth of around 350–400 m (approx). Designed heat load and overall heat transfer co-efficient of the condenser are around 3.4 MW and 1,790 W/m^2 K, respectively, for an inside tube cooling water velocity of 1.25 m/s. The primary objective of this paper is to experimentally study the performance of a shell and tube condenser and to compare it with the HTRI 6.0 results as well as Kern method for the same operating parameters. A comparative study showed that the predicted results of HTRI were in good agreement with experimental values as well as with Kern method. After the comparative study, the reasons for variation in results were identified, reviewed and discussed. Experimental study revealed that the deviation of actual inlet conditions from the design conditions at the plant site greatly influences the condenser performance. It was observed from data analysis that the effect of fouling of deep-sea cooling water on the condenser performance is insignificant. Uncertainty analysis also has been carried out and presented in this paper.

Keywords: Overall heat transfer co-efficient; LMTD; HTRI; Fouling; Condensate; Kern

1. Introduction

Low-temperature thermal desalination plant (LTTD) uses a unique technology in which the surface sea water (28–29°C) is flash evaporated inside a vacuum flash chamber maintained at a pressure of 0.027 bar (abs) at 10.8 m barometric level. The generated vapour from flash chamber reaches a shell and tube condenser through the vapour duct, where it gets condensed to form the product water. The deep-sea cooling water at 12–13°C is drawn from a depth of around 350–400 m using a long high-density poly ethylene (HDPE) pipe of 630 mm OD. Length of the pipe varies between 800 and 1,000 m depending upon the depth profile from the seashore. Two submersible sea water pumps are being used to supply warm surface sea water and deep-sea cooling water to flash chamber and condenser, respectively. Sea water pumps are erected inside a concrete rectangular sump

*Corresponding author.

of size 8 m × 12 m with 9-m height located in 4–5 m water depth. The cooling water pipe is flanged to the sump through a flexible hose for supplying cooling water to the condenser. Vacuum pumps are being used to create and maintain vacuum inside flash chamber and condenser, which is essential for continuous evacuation of non-condensable gases.

In recent years, for most of the engineering applications, the heat exchangers are designed using commercially available software, such as heat transfer and fluid flow service developed by co-operative research, Heat Transfer Research Institute (HTRI) developed by Heat Transfer Research Inc and ASPEN by AspenTech. All these programs offer design and cost analysis for heat exchangers and incorporate multiple design codes and standards from the American Society of Mechanical Engineers (ASME), Tubular Exchanger Manufacturers Association (TEMA) and International Standards Organisation (ISO) [1]. Sahajpal and Shah [2] conducted a comparative study of manual design calculation of ammonia de-superheater condenser with HTRIXchanger suite educational 6.0 software and observed negligible variations in heat duty, number of tubes and shell-side pressure drop. Patel and Mavani [3] presented a new optimization method for evaluating thermal parameters in a single segmental shell and tube heat exchanger water cooler. In this work, HTRI 6.0 version is used for obtaining an optimal mass flow rate and baffle spacing with constant fouling condition of water. Shinde et al. [4] conducted a performance study in terms of pressure drop and shell-side heat transfer co-efficient experimentally and compared it with the HTRI analysis results. Experiments have been conducted in two different heat exchangers, one with segmental baffles and other with helical baffles. The resultant outputs are compared with the analysis results and validated. There is a good agreement between the computational and experimental results. The literature survey reveals that limited papers have been published in the area similar to this work, which involves condensation of low-temperature water vapour (less than ambient temperature) by deep-sea cooling water. In the present study, the computer software HTRI 6.0 version has been used to predict the following technical output parameters of the surface condenser such as overall heat transfer co-efficient, tube side heat transfer co-efficient and bundle side heat transfer co-efficient with respect to the experimentally measured input variables such as cooling inlet and outlet temperatures, cooling water flow rate, mass flow rate of condensate and condenser pressure. The basic objective of this study is to find out how closely the experimental results are matching with theoretical calculation using Kern method and HTRI results for the same input parameters. Also, analysis has been carried out using three-year data to find out the fouling effect of deep-sea cooling water on condenser performance and results have been discussed.

2. Element of surface condenser

Surface condensers are widely used in power plants, chemical industry, refrigeration and air-conditioning plants. Condensers are an integral part of almost all the operations in the process industry. Condensers are basically a heat transfer device which is used to condense a substance from gaseous state to liquid state by cooling it. In common, most of the condensers are using either surrounding air or water as a coolant [5]. Heat transfer mechanism involved in the present work is condensation of the saturated water vapour outside the condenser tubes and transfer of heat to the deep sea water circulating inside the tubes. Operating pressure of the condenser is determined by temperature of the cooling water, mass flow rate of the cooling water and it also depends on the efficiency of the vacuum system. Decrease in the optimum cooling water temperature for reducing condenser pressure results in condensation of large amount of vapour [6]. Decrease in the condenser pressure leads to an increase in the production rate, where the vapour is condensed isothermally if the intrusion of gases such as non-condensable gases (NC) and air is very marginal. Decrease in the cooling water temperature actually helps in reducing the size of air-removal equipment such as vacuum pump by cooling the non-condensable gases [7] and minimizing the vapour-escape rate. An increase in the cooling temperature raises a necessity to increase the mass flow rate, in order to sustain a constant heat load in the condenser for achieving the required production.

3. Mathematical model (Kern method)

Correlations which were used in the thermal calculations are given below:

3.1. Shell-side heat transfer co-efficient (h_o)

Average heat transfer co-efficient based on Nusselt theory for a single horizontal tube is given below [8]:

$$\frac{h_a}{k_l}d = 0.728\left(\frac{\rho_l(\rho_l-\rho_g)gh_{fg}d^3}{(T_{sat}-T_w)k_l\mu_l}\right)^{1/4} \quad (1)$$

where $(T_{sat} - T_w)$ can be obtained by iteration method.

Film condensation in the tube bundle proposed by Kern is as follows [9]:

$$h_o = h_a N^{-\frac{1}{6}} \tag{2}$$

3.2. Tube-side heat transfer co-efficient (h_i)

The correlation proposed by Petukhov [10] is used for estimating the tube-side Nusselt number as follows:

$$\mathrm{Nu}_{tube} = \left(\frac{(f/2)\mathrm{Re}\,\mathrm{Pr}}{1.07 + 12.7(f/2)^{1/2}(\mathrm{Pr}^{2/3} - 1)} \right) \tag{3}$$

where

$$f = (1.58 \ln \mathrm{Re} - 3.28)^{-2} \tag{4}$$

Recommended range of values for Nusselt number is as follows:
$10^4 < \mathrm{Re} < 5 \times 10^6$
$0.5 < \mathrm{Pr} < 200$ with 5–6% error
$0.5 < \mathrm{Pr} < 2{,}000$ with 10% error

$$h_i = \mathrm{Nu}_{tube} \frac{k_{cw}}{d_i} \tag{5}$$

3.3. Overall heat transfer co-efficient (U_o)

The overall heat transfer co-efficient for the surface condenser based on cooling temperature is determined by an iteration procedure as shown in Fig. 1.

Correlations used for calculation are given as follows:

$$\frac{1}{U_o} = R_{th} + \frac{1}{h_o} \tag{6}$$

where R_{th} is the total thermal resistance which can be written as:

$$R_{th} = R_{fo} + \left(\frac{1}{h_o} + R_{fi} \right) \frac{d_o}{d_i} + \frac{t_w d_o}{k_w d_m} \tag{7}$$

$$\Delta T_w = \Delta T - R_{th} q \tag{8}$$

where $\Delta T_w = (T_{sat} - T_w)$, $\Delta T_{ci} = (T_{sat} - T_{ci})$ and $\Delta T_{co} = (T_{sat} - T_{co})$.

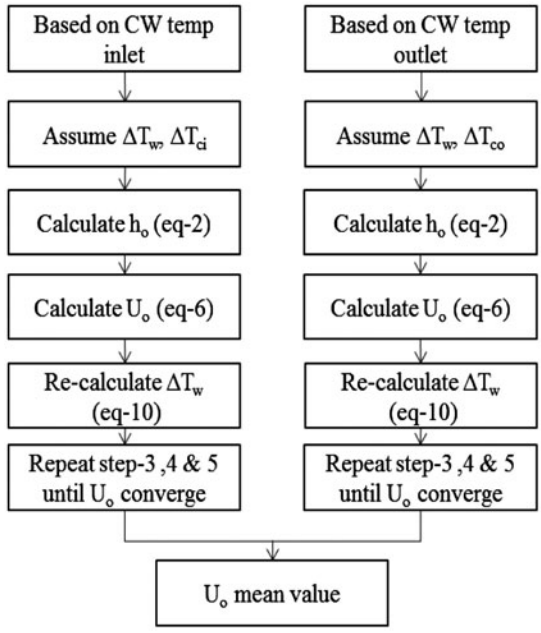

Fig. 1. Iteration procedure.

$$q = U_o \Delta T \text{ [Heat flux]} \tag{9}$$

$$\text{So} \quad \Delta T_w = \Delta T \ (1 - R_{th} U_o) \tag{10}$$

Manual calculation has been done for determining the U_o value based on the iteration method (Fig. 1). The input values for iteration such as saturation temperature, cooling inlet water temperature and cooling outlet water temperature are obtained from the experimental data. U_o experimental value was calculated using the following governing Eq. (11):

$$Q = M_{cw} \ C_{pcw} \ \Delta T_{cw} = U_o \ A \ \text{LMTD CF} \tag{11}$$

3.4. Pressure drop inside tubes (ΔP_{tube})

Pressure drop due to the flow inside condenser tubes is estimated using the number of tube passes, water velocity inside tubes and length of the tubes as given by Eq. (12):

$$\Delta P_{tube} = 4f \frac{L N_p}{2 \rho d_i} G^2 \tag{12}$$

Additional pressure drop due to change in the direction, sudden expansion and contractions is given by the following Eq. (13):

$$\Delta P_{add} = 4N_p \frac{\rho V^2}{2} \quad (13)$$

Total tube-side pressure drop (ΔP_t) can be obtained by summing Eqs. (12) and (13).

4. Experimental set-up and measurement procedure

An experimental study was conducted on a surface condenser of a LTTD plant located at Agatti in UT Lakshadweep group of Islands. In this experiment, the effect of deviation in inlet conditions on the condenser performance was studied. In practical situations, when the desalination plants are installed, there are lot of constraints such as variation in cooling temperature, tide levels and fluctuations in mass flow rates. This leads to an increase or decrease in the plant production and heat transfer rate of condenser. So, the parameters for heat load and production capacity were generated under different conditions of cooling water temperature and mass flow rates.

Based on the site measurement and design data collection, the performance of condenser was evaluated. This evaluation indicated that when the actual inlet condition varied from the design condition, the condenser heat load and production efficiency changed noticeably.

It was observed during plant operation that tidal variation in sea affects the mass flow rate of cooling water as well as warm surface feed water. Friction loss in the demister and vapour duct leads to deviation in the condenser operating pressure from evaporator pressure by 3–5 mbar. Operating pressure of evaporator varies between 24 and 27 mbar, whereas condenser pressure varies between 18 and 22 mbar. When the vapour was reaching the condenser, it would be in a superheated state. This vapour becomes desuperheated by losing its sensible heat to the circulating cooling water and finally condensed to form fresh water at the saturation temperature of the condenser.

4.1. Technical details of the surface condenser

Condenser is basically a shell and tube-type heat exchanger of TEMA—BHM geometry. Water vapour is condensed in the shell side of the condenser and cooling water is circulated in the tube side of the condenser. Condenser's inner diameter is around 1.2 m with 4.88 m tube length. The shell of the condenser is made up of SS304 material. Nearly, 1,120 tubes made up of cupronickel; each of 0.019-m OD and 0.001-m thickness are used for circulating the cooling water. Two-pass arrangements are given in the condenser for an effective condensation of water vapour. The details of the surface condenser are given in Table 1.

The condenser is provided with two temperature transmitters in the common headers for measuring the inlet and outlet cooling water temperatures with an accuracy of ±0.2%. Two vacuum transmitters one in each compartment is installed for the measurement of condenser pressure. Temperature transmitters are provided at the bottom of condenser for measuring the condensate temperature and one is also placed in each side of the shell compartment for measuring the condenser temperature. Flow rate of condensate is measured using vortex type inline flow meter with accuracy of ±1%. Saturation pressure of the condenser is measured using vacuum transmitters (±0.2% accuracy). Flow rate of cooling water is measured using insertion-type flow meter with an accuracy of ±1% (Fig. 2).

5. Study of the effect of deviation of inlet conditions on the condenser performance

5.1. Effect of deviation of inlet cooling sea water temperature on condenser performance

Temperature of cooling water is one of the important parameters for the thermal design of a condenser. It plays a major role in the determination of heat load and effectiveness of the condenser. Performance of the condenser depends on the inlet cooling water temperature available at the plant site condition. Temperature of inlet cooling water is subjected to variation with respect to the ocean currents and seasonal changes in the intensity of solar radiation. Radiation from the sun heats up the surface sea water. Wind and waves mix the surface water from top to bottom. As a result, the heat is transferred downward from the surface in open oceans. Temperature profile of the deep sea is shown in Fig. 3, which shows a decreasing trend in the temperature with an increase in the sea depth [11]. In order to highlight the effect of cooling water temperature on the condenser performance, an observation on temperature variation was done and the corresponding variations happening in the parameters such as heat load, mass flow rate of condensate, condenser pressure and cooling water temperature drop were observed and plotted in Figs. 4 and 5 for clear understanding. Designed inlet cooling temperature for condenser was kept at 12˚C. But, during the plant operation, the temperature of cooling water was varying between 12.2˚C to a maximum of 13.2˚C. Because of this temperature deviation, the condenser heat load was reduced by 11% average (i.e. from 2,550 average

Table 1
Heat exchanger parameters

Item descriptions	Shell side	Tube side
Fluid	Low-temperature water vapour	Deep-sea cooling water
Mass flow rate (kg/s)	1.38	147
Operating pressure (kPa)	2.7	101
Temperature in/out (°C)	22.5/21.5	12.15/17.5
Pressure drop (kPa)	0.5	18
Fouling factor (m^2 K/kW)	0.08	0.08
Material of construction	SS 304	90/10 cupronickel
Tube length (m)	–	4.88
Tube OD (m)	–	0.01904
Tube ID (m)	–	0.01692
Tube thickness (m)	–	0.00106
Tube layout	–	45° square
No of tube passes	–	2
Tube pitch (m)	–	0.02856
Pitch ratio	–	1.5
Baffle cut (%)	25	–
Baffle spacing (m)	0.6	–

Fig. 2. Deep sea water-cooled surface condenser.

to 2,250 kW average) (Fig. 5). Also, it was observed that the temperature drop of cooling water across the condenser tubes decreased by 3.35°C from the design condition of 5.5°C due to the increase in the inlet cooling water temperature by 1.2°C from the design value as shown in Fig. 4.

Discrepancies observed between the design and actual performances of condenser due to the deviation of inlet cooling water temperature at the site are as follows:

(1) Escape water vapour flow rate from the main condenser was increased, which increases the vacuum load.
(2) Heat load due to condensation was decreased.
(3) Heat load of heat exchanger meant for condensing escape water vapour in vacuum system was decreased that affected the performance of vacuum system.
(4) Increase in the condensate temperature and the condenser pressure was observed.

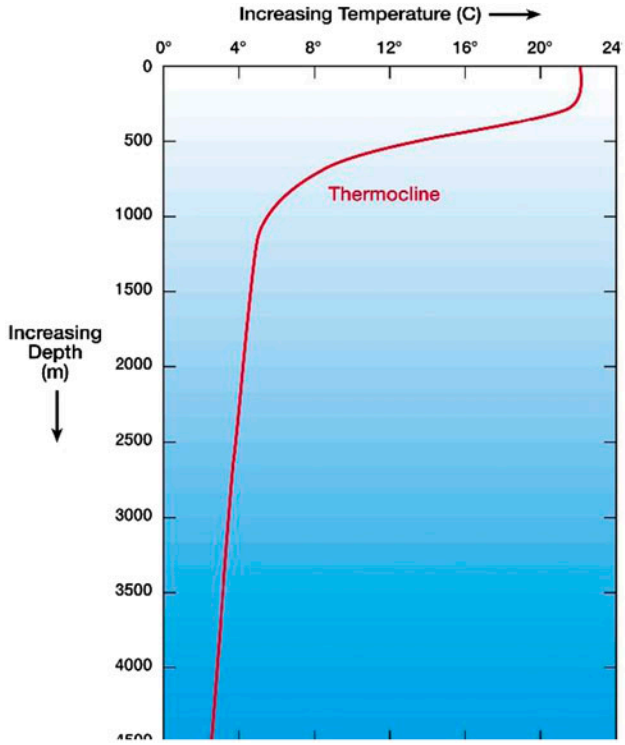

Fig. 3. Temperature profile of deep sea.

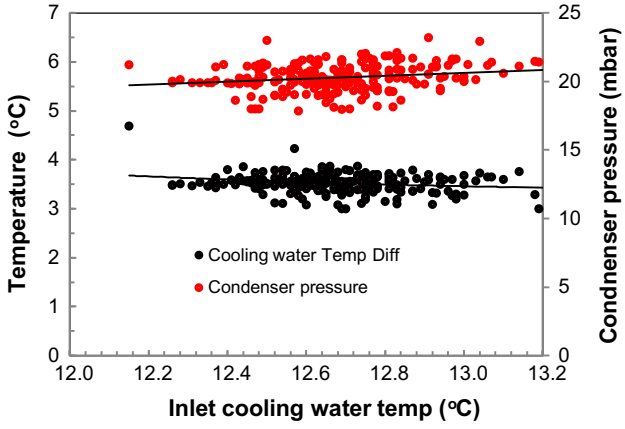

Fig. 4. T_{ci} vs. $\Delta T_{cw}/P_{con}$.

(5) Knocking noise was observed in the condensate pump due to cavitation as a result of increased condensate temperature.

The methods or suggestions to avoid these discrepancies are as follows:

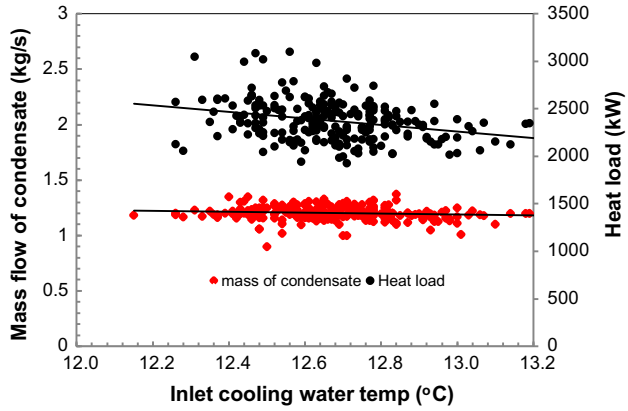

Fig. 5. T_{ci} vs. Q/m_{con}.

(1) Increasing the mass flow rate of cooling water would reduce the escape water vapour rate and improve the condenser heat load to a certain extent.
(2) Increased mass flow rate would improve the heat-carrying capacity of cooling water that can reduce the condensate temperature and its corresponding saturation pressure.
(3) Heat transfer rate of vacuum heat exchanger can be improved by increasing the cooling water flow rate.
(4) Cavitation in condensate pump can be averted by increasing the suction pressure of the pump. This could be done either by increasing the water column height in the suction pipeline of pump or the pump may be lowered further to get an increment in the positive suction head.

5.2. Effect of deviation of mass flow rate of cooling water on condenser performance

In order to highlight the effect of deviation of mass flow rate of cooling water on condenser performance, a study was conducted at different mass flow rates and resultant changes in the calculated output parameters such as heat load and overall heat transfer co-efficient were observed. This study shows that increasing the cooling water flow rate to a maximum of 20% above the design requirement results in an increase in the heat load by 30.4% (Fig. 6) and overall heat co-efficient by 25% (Fig. 7) as shown in Table 2. But these values are found to be relatively lower than the design values.

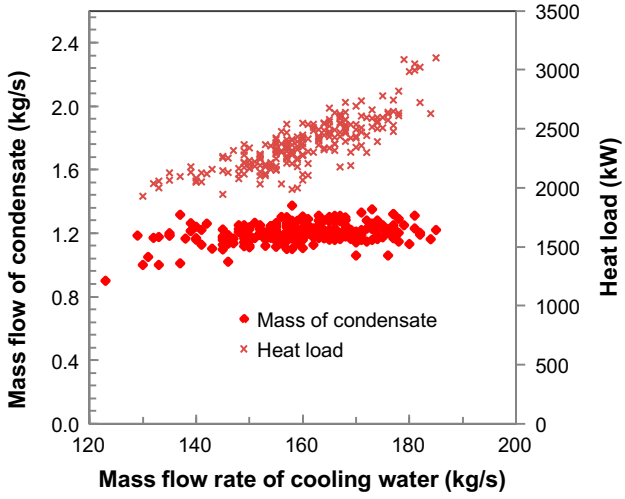

Fig. 6. m_{cw} vs. m_{con}.

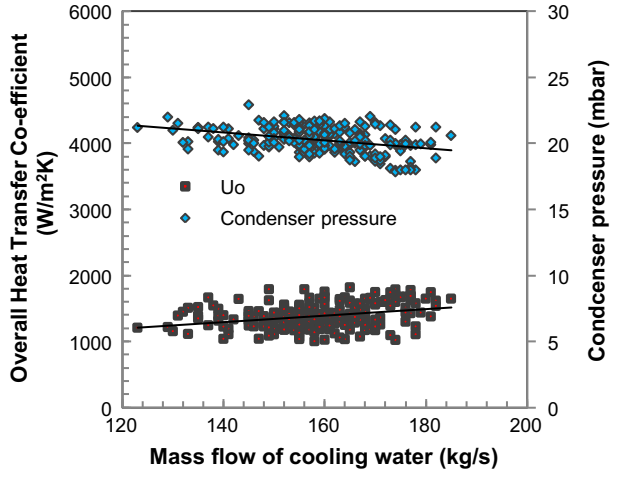

Fig. 7. m_{cw} vs. U_o/P_{con}.

During the experiment, it was observed that an increase in the cooling water flow rate from 147 kg/s to a maximum of 185 kg/s in high tide results in reduction in the condenser pressure by 1.7 mbar (average) (Fig. 7) and an increase in the production rate by 20.7% (Fig. 6) as shown in Table 2.

The present condenser was designed to operate at 147 kg/s mass flow rate of cooling sea water. But in the plant, due to dynamic condition at the site, the flow rate reached up to 185 kg/s, which improved the performance of the condenser.

The discrepancies observed due to the deviation of cooling water mass flow rate from the designed value are as follows:

(1) Increased pressure drop in tubes due to the increased cooling water flow rate resulted in a marginal increase in the power consumption of pump. However, considering the advantages such as increase in the U_o value and yield, the marginal power increment can be neglected.
(2) Increased cooling water mass flow rate may increase the tube erosion and result in tube puncture. However, the percentage of nickel content present in the tubes may resist the erosion to a certain extent. Moreover, Cu–Ni tubes can withstand the flow velocity up to 2.5 m/s.

Benefits of increased mass flow rate of cooling water are as follows:

(1) Increased effectiveness of the condenser.
(2) Increased heat load and heat transfer co-efficient.
(3) No fouling and debris formed in the tubes due to high tube velocity.
(4) Improved performance of the vacuum pump as the service fluid flow rate increases.
(5) Improved performance of the plant as the production rate increases.

6. Daily variation of inlet conditions and output parameters of condenser

Daily fluctuations of the inlet conditions at the plant site such as cooling water inlet temperature and mass flow rate of cooling water are observed and plotted with respect to time in Fig. 8. And also, the corresponding changes happening in the condenser output parameters such as cooling water outlet temperature, condenser pressure, mass flow rate of condensate, heat load, overall heat transfer co-efficient and condensate temperature are recorded and plotted in Figs. 8–10 with respect to time. Tidal variation and change in deep-sea ocean current velocity play a major role in the variation of inlet conditions at the plant site.

7. Comparative study of experimental results, HTRI and Kern method (Table 3)

7.1. Overall heat transfer co-efficient (U_o)—A comparison of experimental result with Kern and HTRI

The overall heat transfer co-efficient (U_o) was calculated based on the experimental data, which shows an increasing trend with an increase in the tube flow velocity as depicted in Fig. 11. For the same experimental input data, the overall heat transfer co-efficient

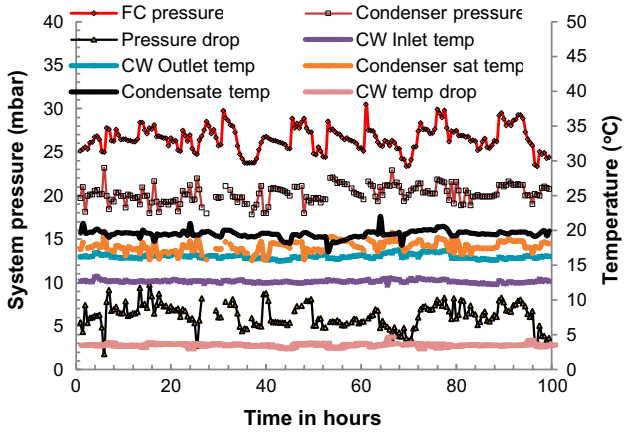

Fig. 8. Inlet and outlet process parameters measured at plant site.

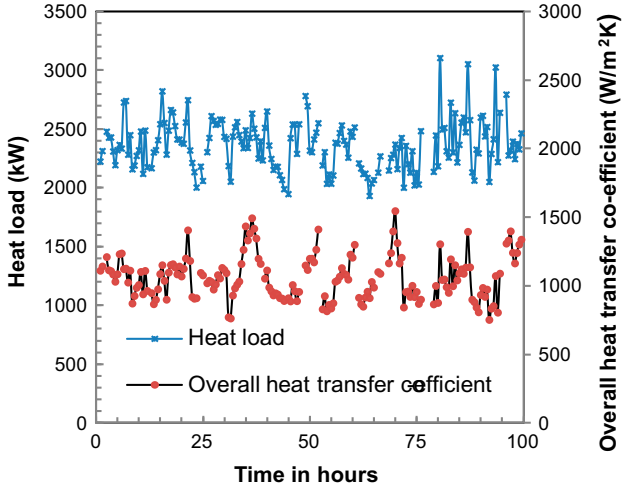

Fig. 9. Time vs. Q, U_o.

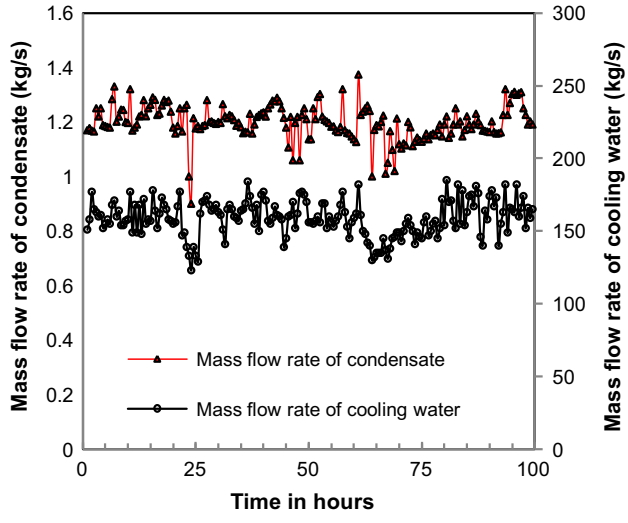

Fig. 10. Time vs. m_{con}, m_{cw}.

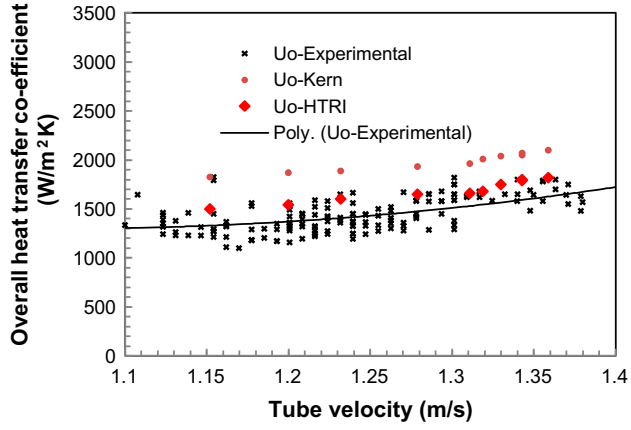

Fig. 11. V_{tube} vs. U_o.

of condenser was estimated using HTRI and Kern method. Both the results were compared with the experimental results. From the comparison, it was found that the results of HTRI and Kern method were matching with the experimental overall heat transfer co-efficient up to 11 and 25%, respectively. HTRI performs design in stepwise and zone-wise modes. In HTRI, cooling water fluid properties are generated by component-by-component method. HTRI includes all the changes that are happening in each zone of the entire condenser. Also, HTRI predicted the results based on the average analysis of all outputs obtained from each of the zone-wise analysis. Hence, HTRI results are closer to the experimental value when compared to Kern method.

The influence of non-condensable gases on the heat transfer co-efficient was not considered in the Kern method. But in the experiment, some amount of NC gases liberated from sea water may present in the shell side of the condenser along with water vapour. This could reduce the heat transfer co-efficient of the condenser. Kern method involves iterative procedure, which includes preliminary assumption such as tube surface temperature that could create some inaccuracy in the calculation, which leads to variation in its results with HTRI and experimental values. The number of tubes obtained from Kern method is 1120, but in HTRI, it is 1086 only; this difference in quantity could be due to the fact that when designing the condenser in HTRI, it considers all mechanical clearances required as per standards. Therefore, for the same pitch ratio, HTRI accommodated lesser tubes than the Kern method.

The effects of the deviation of inlet cooling water temperature, mass flow rate of cooling water and other factors on "U_o" value are as follows:

(1) The heat transfer co-efficient is a function of Reynolds number, Nusselt number and the Prandtl number. Therefore, decrease in the cooling water flow rate resulted in reduced "U_o" value.
(2) An increase in the cooling temperature affects the logarithmic mean temperature difference (LMTD), which in turn reduced the heat load of the condenser and also the "U_o" value.
(3) The factors such as tube blockage and scale formation significantly affect the "U_o" co-efficient value due to reduction in the heat transfer area.
(4) Increased tube fouling also affects the heat transfer co-efficient; however, the present study indicated that fouling did not occur on any of the tubes.

7.2. Shell-side heat transfer co-efficient (h_o)—A comparison between Kern and HTRI

Fig. 12 shows the comparison plot of bundle- or shell-side heat transfer co-efficient of both the Kern method and HTRI calculated based on the experimental input data for different mass flow rates of condensate. Fig. 12 clearly depicts that results predicted by Kern method showed an increase in the heat transfer co-efficient for the corresponding increase in the condensate flow rate compared to HTRI. 18% variation was observed between the results.

Flow character in the shell side is very complex and involves shear of the condensed liquid with water vapour that leads to fluctuation in the vapour velocity within the tube bundle, which is difficult to predict. HTRI considered this aspect for analysing the shell-side heat transfer co-efficient, whereas it was not considered in Kern method. As a result, the heat transfer co-efficient predicted by Kern method was found to be higher than HTRI.

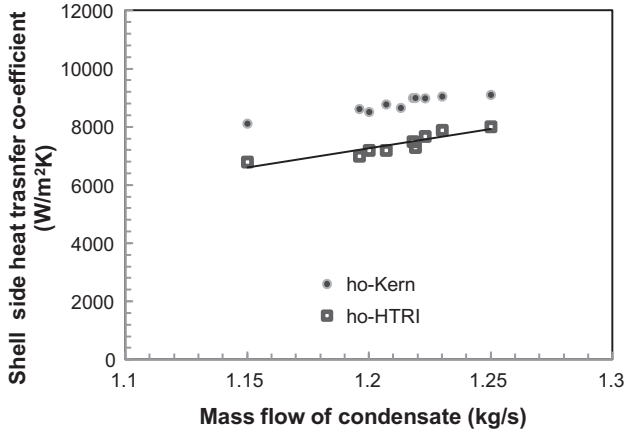

Fig. 12. m_{con} vs. h_o.

Since condenser is handling water vapour in the shell side, the chances for flow induced vibration in the tubes are very high. In order to eliminate the problems caused by the vibration of tubes, the optimum ratio baffle spacing was kept around 0.4 with baffle spacing of 0.6 m for a tube length of 4.88 m and condenser diameter of 1.2 m. As per the guidelines, the optimum ratio of baffle spacing to the shell inner diameter is normally maintained between 0.3 and 0.6. [12]. In order to permit free movement of condensate to the outlet port without any stagnation, the horizontal cut segmental baffles were provided with slots in their bottom portions. This may improve the shell-side heat transfer co-efficient, as condensate stagnation is prevented. The present condenser was designed with TEMA H shell, which has an advantage of less pressure drop in the shell side [12].

Some of the practical observations that could affect the "h_o" values are as follows:

(1) In practical situation, all water vapours flowing across the tubes are not condensed. Some fraction of vapour may escape through clearance between shell and baffles, which may be sucked by the vacuum pump, when they reach near the vacuum suction port before they are condensed to form liquid. This in turn reduces the condenser performance. If sealing strips are introduced in the clearance, the flow fraction could be controlled and heat transfer co-efficient can be improved.
(2) During plant operation, condensate inundation may occur on lower tubes whose effect is to reduce the heat transfer co-efficient of shell-side stream [13].
(3) Portion of tubes between the tube sheet and first baffle on both sides may not be fully reached by the vapour for condensation. Vapour may be diverted to the vacuum suction port before they reach the extreme-end regions of the condenser, this may affect the shell-side heat transfer co-efficient to certain extent. This problem could be avoided either by adjusting the baffle spacing or extending the input vapour duct up to first baffle spacing.
(4) Apart from that, uneven baffle spacing due to fabrication default may also affect the heat

transfer performance of condenser. This requires careful factory inspection during fabrication.

(5) As the condensation of vapour proceeds within the tube bundle, their partial pressure gradually decreases, whereas the NC gas partial pressure increases, this resulted in a reduced saturation temperature of vapour close to inlet cooling temperature that leads to a decreased condenser performance. De-aerator or decarbonizer can be introduced to remove a portion of NC gases before they enter into the process equipment.

(6) Also, an increase in the oxygen content increases the corrosiveness of the condensate in the condenser [14]. This may corrode the tube and reduce the heat co-efficient.

7.3. Tube-side heat transfer co-efficient (h_i) and pressure drop (Δp_{tube})—A comparison between Kern and HTRI

As discussed earlier, the shell side involves a complex procedure for determination of heat transfer co-efficient, where the flow characteristic of the water vapour undergoes a drastic change, when the flow is established through the baffles. Also, the calculation involves an assumption of tube wall surface temperature that leads to the prediction of heat transfer co-efficient by iteration method. But the tube side heat transfer co-efficient involves a simple calculation methodology because the fluid used inside tube is a single-phase fluid that gives results closer to HTRI. Basically, h_i is a function of Reynolds number, Prandtl number and tube diameter. The physical properties such as thermal conductivity, viscosity, specific heat and mass velocity are very important for determining the heat transfer co-efficient value. Variation in liquid viscosity influences the heat transfer co-efficient to a large extent and an increase in the thermal conductivity of liquid promotes a high heat transfer co-efficient [12]. In order to prevent biofouling, a water velocity of more than 1 m/s was maintained inside the tubes. A comparison of results is shown in Fig. 13 with 6% variation. Similarly, pressure drop in condenser tubes gives value very closer to HTRI results as shown in Fig. 14. Mass flow rate of cooling water inside tubes greatly influences the heat transfer co-efficient as well as the pressure drop. But an increase in the mass flow rate increases the pressure drop more quickly than the heat transfer co-efficient value [12]. Therefore, beyond certain point, no advantage is gained by the condenser in increasing the mass flow rate of cooling water. As per the guidelines, the pressure drop permitted in tubes per shell for liquid is 0.5–0.7 bar and for gases,

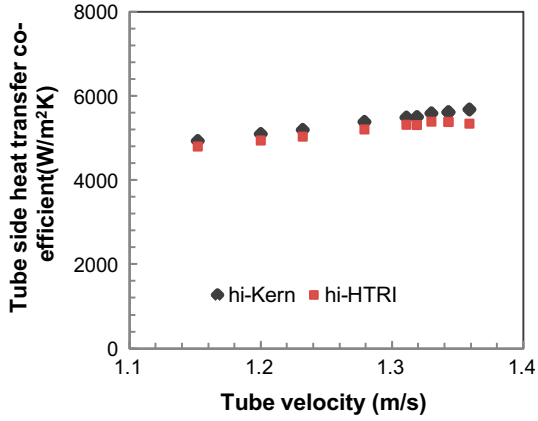

Fig. 13. V_{tube} vs. h_i.

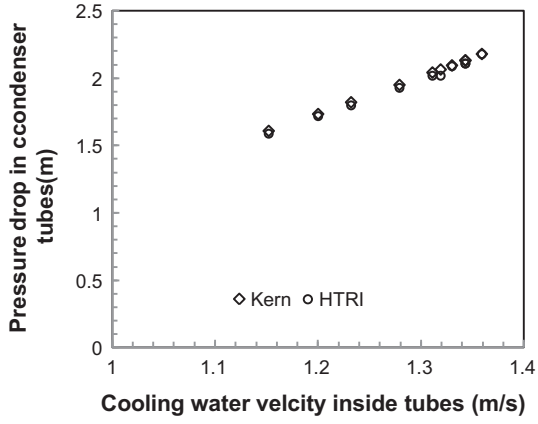

Fig. 14. V_{tube} vs. Δp_{tube}.

it is 0.05–0.2 bar [12]. Pressure drop calculation was done based on experimental input data such as mass flow rate and temperature of the cooling water. The results are portrayed in Fig. 14, which indicated a variation of 5% between the calculated and HTRI values.

8. Condenser tube fouling

Fouling in the condenser tubes causes a significant economic problem in both thermal power plants as well as in thermal desalination plants, and the reduced heat transfer capability in the condenser due to fouling results in a decreased production rate of distillate in the desalination plant and reduced power output in the power plants as a result of high back pressure in the condenser [15]. Fouling of condenser tubes generally occurs due to the factors such as microbiological growth, scale formation, deposition of

debris, corrosion of condenser tube material and blockage of tube sheets, and even a thin layer of fouling formed by microbiological growth affects the heat transfer process significantly [15].

A physical observation was carried out on the existing condenser tubes, but did not find any sign of biofouling growth on the tube surface as shown in Fig. 15. Scaling is mostly promoted by the elevated temperature existing in the wall surface of the condenser tubes, but in the present case, it is not a problem because the operating temperature of the condenser at any point of time varies between 20 and 24°C only. Generally, particle deposition occurs in tubes when the cooling water flow rate is inadequate, but in the existing condenser, deep-sea cooling water was circulated inside tubes which were free of suspended particles. However, during physical observation, some soil sediments were seen which are of very small quantities. These sediments were present inside the concrete sumps, where the sea water pump was placed to discharge the cooling water. During the water turbulence, these sediments got disturbed and carried by water to the condenser tubes.

No chemicals were used in the circulating cooling water of condenser. Chemicals include biocides for controlling the growth of micro-organisms, antiscalants for the control of scale formation, dispersants for the settling of suspended particles and corrosion inhibitors for the control of corrosion in tube materials, which are generally applied in desalination and power plants. Generally zinc, and phosphate are used as an inhibitor for carbon steel tubes and triazoles used for copper alloys [15]. Blockage of the tube sheet by any of the debris like papers, wooden pieces and aquatic animals such as fish is avoided by putting water screens made of SS304 material.

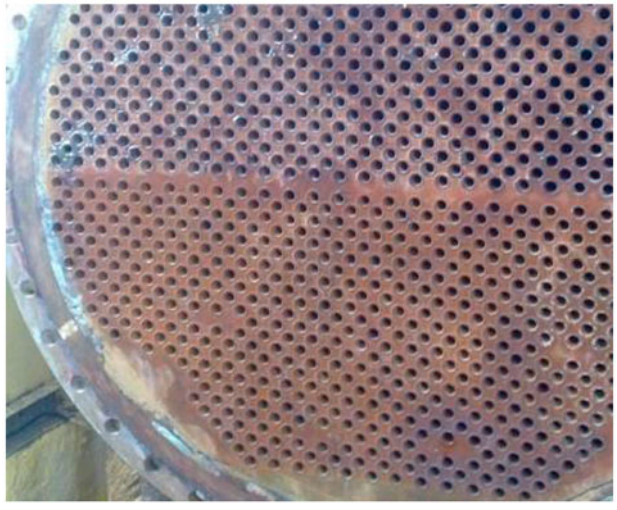

Fig. 15. Picture of condenser tubes.

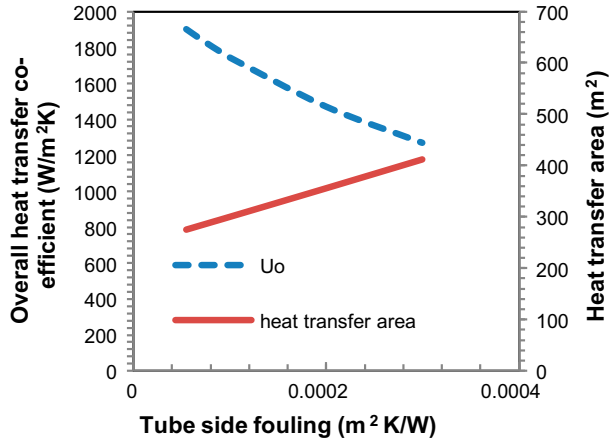

Fig. 16. R_{fi} vs. U_o/heat transfer area.

In order to highlight the significance of the effect of fouling on the condenser tubes, a calculation was done on the heat transfer area as well as overall heat transfer co-efficient of the condenser for different fouling factors as shown in Fig. 16. The present condenser was designed using a fouling factor of around 0.088 m^2 K/kW. As the fouling factor increases, the heat transfer area required for maintaining a constant heat load also increases and the overall heat transfer co-efficient of the condenser decreases, which is depicted in Fig. 16. But for the present condenser, the effective heat transfer area was not affected by fouling, since no fouling was observed in condenser tubes as shown in picture 16. In case, if biofouling is formed on the condenser tubes, then the effective heat transfer area available for condensation would be considerably reduced that resulted in decreased overall heat transfer co-efficient and heat load. Performance analysis of condenser for the last three years is shown in Figs. 17 and 18 for overall heat transfer co-efficient and mass flow rate of condensate, respectively. It was observed that the heat transfer co-efficient and production rate of the condenser did not show any large variation in the last three years. This could be due to no formation of fouling on the tubes, since the condenser is running at a low operating temperature of the range 12–13°C.

9. Results and discussions

Based on the experimental study conducted on the surface condenser, the following observations were made:

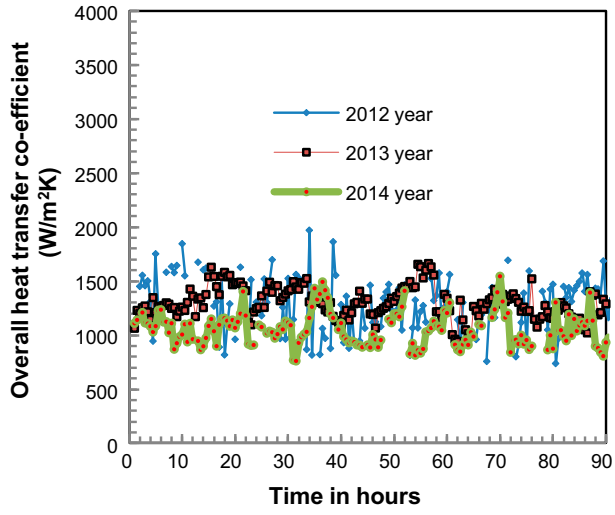

Fig. 17. Time vs. U_o.

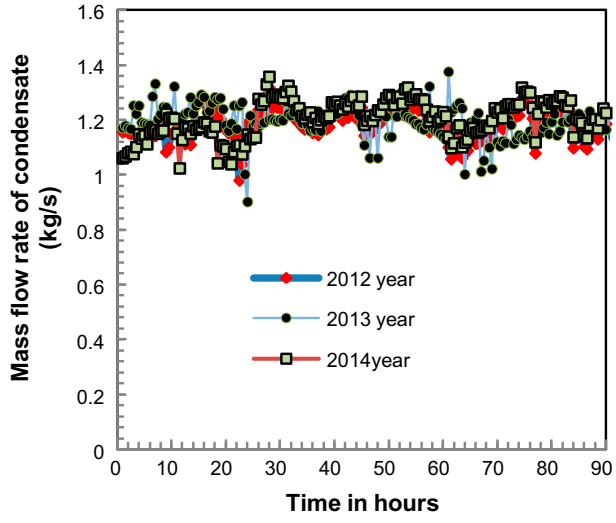

Fig. 18. Time vs. m_{con}.

(1) Deviation of inlet conditions (at site) from design conditions greatly influences the condenser performance.
(2) Deviation of inlet cooling temperature by 1.2℃ i.e. 10% results in reduction in the heat load by 27.9%, production rate by 20.2% and overall heat transfer co-efficient by 16%, which is shown in Table 4. As the cooling water temperature raised, the quantity of vapour getting condensed decreases. This could be due to reduction in the heat-carrying capacity of cooling water.
(3) It is depicted in Fig. 19 that as the cooling temperature increased by 1.2℃, the condenser pressure raised by 1.10 mbar. This could be due to reduction in heat transfer rate as a result of decrease in the partial pressure of vapour and its corresponding saturation temperature, whereas the other part, such as NC gas experiences an increment in the partial pressure, which further resists the condensation process near the surface of the tubes.
(4) Maximum heat load observed in condenser during the experiment was around 3 MW for a maximum flow rate of 185 kg/s at a cooling water temperature of 12.2℃.
(5) It was observed from experiment that even after increasing the mass flow rate of cooling water by 20% above design requirement, the heat load of condenser could not be increased to its full capacity. This could be due to the measured cooling water temperature at the plant site, which was always found to be greater than design temperature. The present condenser was designed for 3.4 MW with cooling temperature of 12℃. But at the site, the measured cooling temperature varied between 12.2 and 13.2℃ throughout the day.
(6) Increased mass flow rate of cooling water above the design condition made the condenser to operate at 88.7% of its designed heat load, 88.5% of its designed production rate and 92.2% of its designed overall heat transfer co-efficient.
(7) Experimental results showed that the overall heat transfer co-efficient was found to be maximum compared to heat load and production rate. This could be because of consideration of fouling factor of 0.088 m^2 K/kW for heat transfer co-efficient calculation. Physical observation indicated that the deep-sea cooling water circulated inside tubes produced a negligible fouling effect.
(8) It is depicted in Fig. 20 that as the cooling water mass flow rate increased, the condenser pressure decreased by 1.2 mbar. This could be due to the removal of more amount of heat from vapour by condensation. Because of this, the shell-side saturation temperature is decreased that in turn reduces condenser pressure.
(9) It was observed from the data collected at the plant site that the daily average variation of the cooling water temperature from design was around 1.6% and went up to a maximum of 10%.

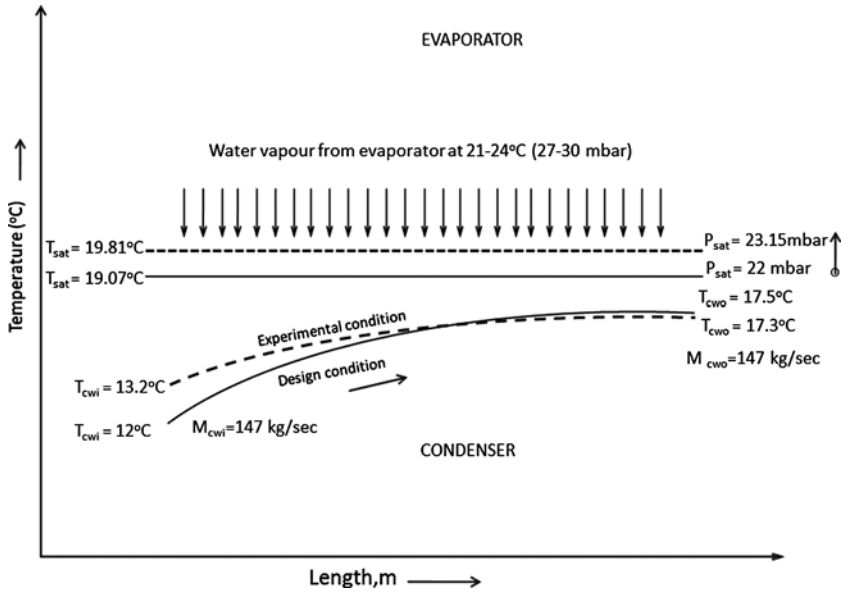

Fig. 19. Observed process condition when cooling water temperature deviated from design value.

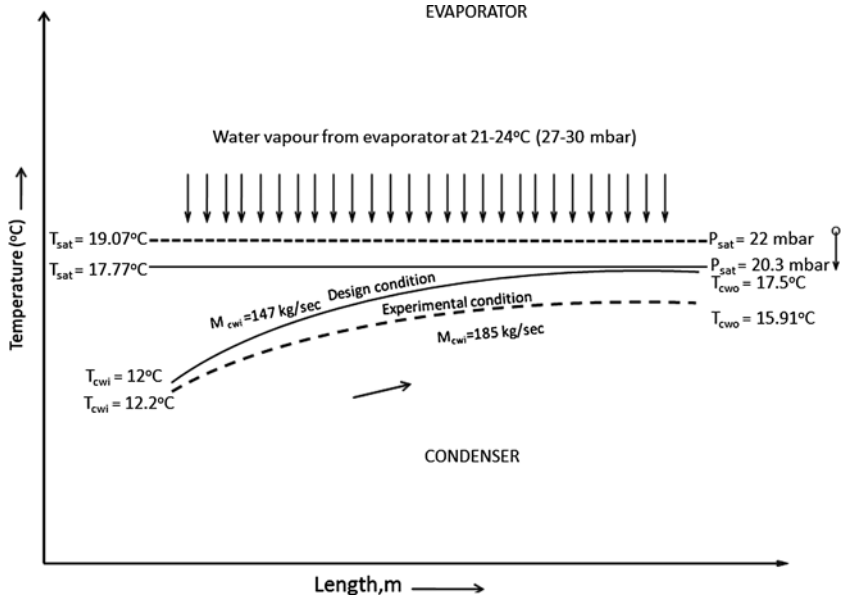

Fig. 20. Observed process condition when cooling mass flow rate deviated from design value.

Table 2
Effect of mass flow rate of cooling water on condenser performance

Parameters	Design values	Experimental values		% difference
Cooling water flow rate (kg/s)	147	147	185	20
Heat load (kW)	3,400	2,300	3,000	30.4
Overall heat transfer co-efficient (W/m^2 K)	1,790	1,320	1,650	25
Mass flow of condensate (kg/s)	1.38	1.01	1.22	20.7

Table 3
Comparative analysis of Kern method, HTRI and experimental

Parameters	Kern method	HTRI	Experimental
Type of exchanger	BHM	BHM	BHM
Shell ID (m)	1.2	1.2	1.2
No of tubes	1,120	1,086	1,120
Heat transfer area (m^2)	296	313	296
Heat duty (kW)	3,398	3,358	3,000
Shell side			
Mass flow (kg/s)	1.38	1.37	1.22
Pressure drop Δp (kPa)	0.5	0.227	–
Heat transfer co-efficient	8,464	7,868	–
Tube side			
Velocity	1.23	1.21	1.38
Pressure drop Δp (kPa)	16.82	16.33	–
Heat transfer co-efficient (W/m^2 K)	4,980	4,870	–
Overall heat transfer co-efficient (W/m^2 K)	1,790	1,774	1,650
Percentage of overdesign (%)	–	7.06	

Based on the comparative study of the surface condenser between Kern method, HTRI and experimental results, the following observations were made:

(1) Overall heat transfer co-efficient: it was found that the experimental results were in a good agreement with HTRI and both results were matching up to 11%. But when comparing the experimental results with the Kern method, it was matching up to 25% only. HTRI does design in stepwise and zone-wise modes. It follows rigorous and integral approach which produces accurate results compared to manual predictions by Kern method which could be inaccurate due to human error.
(2) Shell-side heat transfer co-efficient: in practical scenario, condensed liquid as well as vapour and also a quantity of NC gases would be present in the middle of tube bundle during condensation process. But theoretical calculations were performed on the assumption that all the vapour would be condensed to form liquid with no presence of non-condensable gases. Similarly for HTRI analysis, the effect of non-condensable gas was not considered. However, Kern method over predicts heat transfer co-efficient by 18% compared to HTRI values. This could be due to the assumptions made in theoretical calculations such as skin temperature of the tube on shell side, which was estimated by iteration method and also due to adoption of a single-point average temperature for overall calculations.
(3) Tube-side heat transfer co-efficient: close agreement was found between Kern method and HTRI results. Tube-side heat transfer co-efficient involves single-phase flow that follows a simple methodology for calculation. As a result, the Kern method predicts heat transfer co-efficient closer to HTRI results.
(4) Tube-side pressure drop: Kern method predicted the tube-side pressure drop closer to the HTRI results. This could be because of the calculation procedure for estimating pressure drop in straight tubes which is relatively simple compared to shell side.

10. Experimental uncertainty

Experimental results are subjected to errors due to instrumentation accuracies, measurement techniques, limitations of experimental facilities, environmental variability, etc. [16]. Deviation between measured value and true value is termed as error. Since the true value is generally unknown, the error made in the experimental values cannot be determined. Therefore, to quantify the goodness of the experiment result, a concept of "Uncertainty" was developed.

The input parameters for calculating the uncertainty are given in Table 5.

The overall heat transfer co-efficient was calculated using Eq. (14). In this equation, ΔT_{lmtd} is the LMTD. LMTD can be calculated from the inlet cooling water temperature, the cooling discharge water temperature from the condenser and saturation temperature of the shell side of condenser using Eq. (15) (Table 6).

Table 4
Variations in condenser performance as a result of deviation in inlet conditions

Cooling water temp (T_{ci}) (°C)		Deviation in temp (T_{ci}) (°C)	Cooling water flow (m_{cw}) (kg/s)		Production rate (m_{con}) (kg/s)		% variation in production rate	Overall heat transfer co-efficient (U_o) (W/m^2 K)		% variation U_o	Heat load (Q) (MW)		% variation in heat load	LMTD (°C)	
Dsgn	Exp		Dsgn	Exp	Dsgn	Exp		Dsgn	Exp		Dsgn	Exp		Dsgn	Exp
Deviation of cooling water temperature from the design conditions															
12	13.2	1.2	147	147	1.38	1.10	20.2	1,790	1,502	16	3.4	2.45	27.9	7	6.1
Deviation of cooling water mass flow rate from the design conditions															
12	12.2	0.2	147	185	1.38	1.22	11.5	1,790	1,650	7.8	3.4	3.0	11.7	7	7.1

Table 5
Input parameters for uncertainty calculation

Avg. temperature of inlet cooling water (℃)	12.5	±0.2%
Avg. temperature of outlet cooling water (℃)	17	±0.2%
Avg. saturation temperature of shell side (℃)	20	±0.2%
Avg. mass flow rate of cooling water (kg/s)	160	±1%

Table 6
Average uncertainties of various parameters

S. no.	Parameters	Values in %
1	LMTD	±8
2	Cooling water mass flow rate (m_{cw})	±1.6
3	Heat transfer rate of cooling water (q_{cw})	±32.5
4	Overall heat transfer co-efficient (U_o)	±28.5

$$U_{\text{Overall}} = \left(\frac{q_{\text{cw}}}{\Delta T_{\text{LMTD}}}\right) \tag{14}$$

$$\Delta T_{\text{LMTD}} = \left(\frac{(T_{\text{sat}} - T_{\text{cwi}}) - (T_{\text{sat}} - T_{\text{cwo}})}{\ln \frac{T_{\text{sat}} - T_{\text{cwi}}}{T_{\text{sat}} - T_{\text{cwo}}}}\right) \tag{15}$$

The heat load was determined from an energy balance in the cooling water given by Eq. (16), which is a function of mass flow rate, specific heat capacity and inlet and outlet temperature differences.

$$q_{\text{cw}} = m_{\text{cw}} C_{\text{pcw}} (T_{\text{cwo}} - T_{\text{cwi}}) \tag{16}$$

The following Eqs. (17) and (18) were used to estimate uncertainties for LMTD and heat transfer rate of cooling water, respectively [16].

$$u(\Delta T_{\text{lmtd}}) = \sqrt{\left(\frac{\partial \Delta T_{\text{lmtd}}}{\partial T_{\text{sat}}} u(T_{\text{sat}})\right)^2} + \sqrt{\left(\frac{\partial \Delta T_{lmtd}}{\partial T_{\text{cwi}}} u(T_{\text{cwi}})\right)^2} + \sqrt{\left(\frac{\partial \Delta T_{\text{lmtd}}}{\partial T_{\text{cwo}}} u(T_{\text{cwo}})\right)^2} \tag{17}$$

$$u(q_{\text{cw}}) = \sqrt{\left(\frac{\partial q_{\text{cw}}}{\partial m_{\text{cw}}} u(m_{\text{cw}})\right)^2} + \sqrt{\left(\frac{\partial q_{\text{cw}}}{\partial T_{\text{cwi}}} u(T_{\text{cwi}})\right)^2} + \sqrt{\left(\frac{\partial q_{\text{cw}}}{\partial T_{\text{cwo}}} u(T_{\text{cwo}})\right)^2} \tag{18}$$

After estimating the uncertainties in the LMTD and q_{cw}, the uncertainty in the U_o can be calculated by Eq. (19):

$$u(U_{\text{overall}}) = \sqrt{\left(\frac{\partial U_{\text{overall}}}{\partial T_{\text{lmtd}}} u(\Delta T_{\text{lmtd}})\right)^2} + \sqrt{\left(\frac{\partial U_{\text{overall}}}{\partial q_{\text{cw}}} u(q_{\text{cw}})\right)^2} \tag{19}$$

11. Conclusions

The analysis of surface condenser has been carried out using Kern method as well as with HTRI 6.0 version software and compared with experimental results. It was observed that most of the results obtained by Kern method and HTRI were matching with the experimental results. Marginal variations were observed in overall heat transfer co-efficient and shell-side heat transfer co-efficient. Very close agreement was observed for tube-side heat transfer co-efficient and tube-side pressure drop of surface condenser. It was also found from the experiment that the deviation of inlet conditions at the plant site such as cooling temperature significantly affects the condenser performance. Deviation of inlet cooling temperature by 8.3% from designed condition results in reduction in the heat load by 27.9%, production rate by 20.2% and overall heat transfer co-efficient by 16%. Similarly, deviation i.e. increment in the mass flow rate of cooling water above the designed condition by 20% made condenser to operate at 88.7% of its designed heat load, 88.5% of its designed production rate and 92.2% of its designed overall heat transfer co-efficient. Experimental observation reveals that no fouling was seen in condenser tubes even after continuous operation of plant for 3 years. An uncertainty analysis has been carried out, which indicated the uncertainty in the heat transfer rate of cooling water and overall heat transfer co-efficient of condenser as ±32.5 and ±28.5%, respectively.

Nomenclature

T_{sat} — saturation temperature of condenser (K)
T_{ci} — cooling water inlet temperature (K)
t_{w} — tube thickness (m)
Q — heat load (kW)
q — heat flux (kW/m^2)
μ_{l} — dynamic viscosity of liquid (N s/m^2)
k_{w} — thermal conductivity of tube (W/m/K)
N_{P} — no of tube passes
k_{l} — thermal conductivity of liquid (W/m/K)
Nu — Nusselt number
ρ_{g} — density of vapour (kg/m^3)
V — tube velocity (m/s)
G — mass velocity (kg/m^2/s)
ρ_{l} — density of liquid (kg/m^3)
f — friction factor
Re — Reynolds number

Pr — Prandtl number
d_o — outer diameter of tube (m)
d_m — mean diameter of tube (m)
R_{th} — total thermal resistance (m^2 K/W)
U_o — overall heat transfer co-efficient ($W/m^2/K$)
d_i — inner diameter of tube (m)
M_{CW} — mass flow rate of cold sea water (kg/s)
h_i — tube heat transfer co-efficient ($W/m^2/K$)
h_o — shell heat transfer co-efficient ($W/m^2/K$)
R_{fi} — fouling factor inside tubes (m^2 K/W)
R_{fo} — fouling factor outside tubes (m^2 K/W)
h_a — Avg. heat transfer co-efficient ($W/m^2/K$)
h_{fg} — latent heat of condensation (kJ/kg)
ΔP_{tube} — tube-side pressure drop in condenser (m)
ΔT_{cw} — cooling water temp difference (K)
T_w — wall temperature (K)
m_{con} — mass flow rate of the condensate (kg/s)
T_{co} — cooling water outlet temperature (K)
P_{con} — condenser pressure in shell side (mbar)
u_{cw} — uncertainty in cooling sea water (%)
$u(q_{cw})$ — uncertainty in cooling sea water (%)
$u(U_{overall})$ — uncertainty in overall heat transfer co-efficient(%)
$u(\Delta T_{lmtd})$ — uncertainty in LMTD (%)
$u(m_{cw})$ — uncertainty in cooling water mass flow rate (%)
$u(T_{sat})$ — uncertainty in saturation temperature of condenser(%)
$u(T_{cwi})$ — uncertainty in cooling inlet water temperature (%)
$u(T_{cwo})$ — uncertainty in cooling outlet water temperature (%)

Subscripts

LTTD — low-temperature thermal desalination
OD — outer diameter
ID — inner diameter
HRTI — Heat Transfer Research Institute
ASME — American Society of Mechanical Engineers
TEMA — Tubular Exchange Manufacturing Association
ISO — International Organization for Standardization
HDPE — high-density poly ethylene
LMTD — logarithmic mean temperature difference
NC gas — non-condensable gas
UT — union territories
CF — correction factor
N — no of tube arrays
N_P — no of tube passes

References

[1] K.C. Leoug, K.C. Toh, Y.C. Leong, Shell and tube heat exchanger design software for educational applications, Int. J. Eng. Edu. (14.3) (1998) 217–224.
[2] S. Sahajpal, P.D. Shah, Thermal Design of Ammonia Desuperheater-Condenser and Comparative Study with HTRI, Elsevier 51 (2013) 375–379.
[3] K. Patel, A.M. Sandeep, Mavani, A new optimization method for evaluating thermal parameters in a single segmental shell and tube heat exchanger, IJETED 3(2) (2013) 648–655.
[4] S.S. Shinde, S.S. Joshi, S. Pavithran, Performance improvement in single phase tubular heat exchanger using continuous helical baffles, Int. J. Eng. Res. Appl. 1(2) (2012) 1141–1149.
[5] V. Haldkar, A.K. Sharma, R.K. Ranjan, V.K. Bajpai, Parametric analysis of surface condenser for thermal power plant, Int. J. Therm. Technol., ISSN 2277-4114 3 (4) (2013)155–159.
[6] P. Sharma, S.P.S. Rajput, M. Pandey, Exergetic optimization of inlet cooling water temperature of cross flow steam condenser, Int. J. Emerg. Technol. 2(1) (2011) 144–147.
[7] A.S. Sikarwar, D. Dandotiya, S.K. Agrawal, Performance analysis of surface condenser under various operating parameters, Int. J. Eng. Res. Appl. (3.4) (2013) 416–421.
[8] W. Nusselt, The condensation of steam on cold surface, Z. d. Ver. Deut. Ing (60) (1916) 541–546.
[9] D.Q. Kern, Mathematical development of tube loading in horizontal condensers, AIChE J. 4(2) (1958) 157–160.
[10] B.S. Petukhov,Heat transfer and friction in turbulent pipe flow with variable physical properties, in: T.F. Irvine, J.P. Hartnett (Eds.), Advances in Heat Transfer, vol. 6, Academic Press, New York, NY, 1970, pp. 504–564.
[11] http://www.windows2universe.org/earth/Water/temp.html.
[12] R. Mukherjee, Effectively design shell and tube heat exchangers, Chem. Eng. Prog. 94(2) (1998) 21–37.
[13] T. Murase, H.S. Wang, J.W. Rose, Effect of inundation for condensation of steam on smooth and enhanced condenser tubes, Int. J. Heat Mass Transfer 49 (2006) 3180–3189.
[14] R.K. Kapooria, S. Kumar, K.S. Kasana, Technological investigations and efficiency analysis of a steam heat exchange condenser: Conceptual design of a hybrid steam condenser, J. Energy South Africa 19(3) (2008) 35–45.
[15] G.H. Andrew Jr., E.S. George, Condenser tube fouling and failures: Cause and mitigation, Power Plant chemistry, ISSN 1438-5325 7(12) (2005) 707–717.
[16] F.J. Uhía, A. Campo, J. Fernández-Seara, Uncertainty analysis for experimental heat transfer data obtained by the Wilson plot method: Application to condensation on horizontal plain tubes, Therm. Sci. 17(2) (2013) 471–487.